Desalination and Water Treatment
www.deswater.com

doi: 10.1080/19443994.2015.1036465

57 (2016) 10802–10814
May

Taylor & Francis
Taylor & Francis Group

Supported iron oxide onto an Iranian clinoptilolite as a heterogeneous catalyst for photodegradation of furfural in a wastewater sample

Sakineh Mousavi-Mortazavi, Alireza Nezamzadeh-Ejhieh*

Department of Chemistry, Shahreza Branch, Islamic Azad University, P.O. Box 311 86145, Shahreza, Isfahan, Iran, Tel. +98 31 53292531; Fax: +98 31 53291018; email: sa.mortzavi@gmail.com (S. Mousavi-Mortazavi), Tel. +98 31 53292515; email: arnezamzadeh@iaush.ac.ir (A. Nezamzadeh-Ejhieh)

Received 10 May 2014; Accepted 27 March 2015

ABSTRACT

FeO-clinoptilolite was prepared and characterized by Fourier transformation infrared, X-ray diffraction, X-ray photoelectron spectroscopy, thermogravimetry, scanning electron microscope, and transmission electron microscope techniques and then it was used in the photodegradation of furfural ($C_5H_4O_2$) in a wastewater sample under Hg-lamp irradiation. The degradation extent was monitored by UV/V by absorption spectroscopy, chemical oxygen demand (COD), and high-performance liquid chromatography. Based on the results, the efficiency of the process significantly depended on the experimental factors, so the best degradation extent of the pollutant was obtained at: pH 8, 4 g L^{-1} of the catalyst, irradiation time of 120 min, 50 mmol/L H_2O_2, and 50 mg/L $KBrO_3$. A decrease of COD up to 45% was observed after 120 min irradiation of the sample.

Keywords: FeO; Clinoptilolite; Heterogeneous catalysis; Furfural; Wastewater

1. Introduction

Many industrial effluents contain considerable amounts of organic compounds. Discharge of these hazardous compounds to water without prior treatment causes havoc to the ecological balance in the environment, because these compounds have a long life in natural environment [1,2]. Among important organic compounds in industrial wastewater, furfural is a good example; it is harmful in contact with skin, toxic when it is inhaled or swallowed, and also shows some limited carcinogenic effects [3,4]. It can be easily absorbed through the skin and must not be released into sewer and water bodies [5]. This compound has been used as a solvent for extractive refining of lubricating oils, as it is very effective for removing compounds containing oxygen or sulfur [6]. Furfural is one of the major feedstock for producing furfuryl alcohol, which is used for making resins, and tetrahydrofuran as an excellent solvent. This volatile organic compound is one of the major components of wastewater of petrochemical industry and petroleum refineries. The separation of furfural is an important field of study for the sake of industrial safety and environmental protection [7].

Among the various methods for removing of different pollutants from water and wastewater, advanced oxidation processes are the most famous methods based on the generation of very reactive species such as hydroxyl radicals [8]. Heterogeneous

*Corresponding author.

photocatalytic reactions take place when a semiconductor particle absorbs a photon of light more energetic than its band-gap energy [9]. This excitation generates the holes that react with adsorbed hydroxyl species or water molecules, thereby producing reactive hydroxyl radicals which can degrade non-selectively a broad range of organic pollutants. On the other hand, hydroxyl radical can oxidize almost all organic matters and mineralize them to carbon dioxide and water owing to its high oxidation potential [8–10]. Several attempts have been made to improve the photo-efficiency of different semiconductors by supporting them onto suitable supports such as: silica, alumina, zeolites, clays, and activated carbon [11].

Zeolites modified with transition metal cations have been paid more attention as promising catalysts for a variety of important reactions [12]. Zeolites have been widely used in separation and refinery industries as catalysts, adsorbents, and ion exchangers. The significant catalytic activity and selectivity of zeolites are attributed to the large internal surface area and highly distributed active sites that are accessible through uniform pores size, high thermal stability, chemical inertness, and high mechanical strength. Clinoptilolite, with sedimentary rocks of volcanic origin, is the most abundant natural zeolite in Iran [13,14].

In this work, using of an Iranian natural clinoptilolite (CP) as an abundant, accessible, and cheap material reduces the cost of the method. After purification of the powdered zeolite, ion exchange process was carried out in a Fe(II) solution and the obtained Fe-clinoptilolite (Fe-CP) sample was calcined to produce FeO-clinoptilolite (FeO-CP). The obtained composite was used as a photocatalyst for the degradation of furfural in a wastewater solution. The photocatalytic degradation of organic pollutants on the surface of iron oxides is very feasible and useful to remove organic pollutants from contaminated soils and waters [15,16]. In our previous work, similar wastewater sample was degraded by NiS-clinoptilolite [12] and the optimal operation parameters were obtained as: pH 5, 330 mg/L^{-1} of the catalyst dosage and 6 mmol/L of furfural concentration. But, the optimal conditions in this work are: pH 8, 4 g/L^{-1} of the catalyst and 37.5 mmol/L of furfural concentration. In the present work, 50% of a 37.5 mmol/L was degraded while 45% of 6 mmol/L furfural was degraded in our previous work [12]. We believe that due to ever-increasing pollution of water from industrial wastewaters, it is important to focus the photodegradation researches to wastewater cleaning. Hence, a furfural wastewater sample was subjected in this work instead of a common synthetic one.

2. Experimental

2.1. Materials

Natural CP (belongs to the Semnan region in the northeast of Iran) was prepared from Afrand Tuska Company (Isfahan, Iran). Furfural (molecular formula, $C_5H_4O_2$; molecular weight, 96.09 g/mol^{-1}; characteristic, 254 nm; LD50, 65 mg/kg; bp (11 Torr), 54–56 °C; density, 1.159 g/mL^{-1}), ferrous sulfate heptahydrate, hydrogen peroxide (H_2O_2), sodium hydroxide, hydrochloric acid, potassium bromate ($KBrO_3$) were obtained from Merck Company. Distilled water was used throughout the experiments. The pH of the solutions was appropriately adjusted with sodium hydroxide or hydrochloric acid solution. The used industrial wastewater was obtained from Isfahan Oil Refinery Company and its characteristics are shown in Table 1. The used wastewater was only pretreated by simple filtration for removing of any suspended solids.

2.2. Preparation of FeO-CP

In the first step the raw CP was mechanically pretreated, by crushing in an agate mortar and sieving in analytical sieves, for separating the particles with sizes smaller than 100 μm. For removing water soluble impurities, aqueous suspension of the obtained powder was heated at 70 °C for 8 h ($n = 3$). In order to reach fixed water content, after filtration, washing, and drying, the purified material was stored in a desiccator over saturated sodium chloride solution for two weeks.

To prepare FeO-CP, 10 g of the pretreated powder was added to 100 mL 0.2 mol/L $FeSO_4.7H_2O$ aqueous solution in a polyethylene bottle and shaken for 8 h at a fixed agitation speed of 350 rpm at room temperature. The procedure was repeated again to complete ion exchange process. The sample was filtered, washed with water, and dried at 110 °C. Finally, the sample was calcined at 450 °C for 8 h and the obtained material was referred as FeO-CP. Other FeO-CP catalysts were prepared by the same method in 0.1 and 0.5 mol/L Fe(II) solutions.

Table 1
Characteristics of original wastewater sample

Parameter	Average value (mg/L^{-1})
Furfural	375
TSS	189
TOC	1,450
COD	134

2.3. Characterization of samples

The X-ray diffraction (XRD) patterns of samples were recorded using a Bruker diffractometer (D8 Advance) with a Ni-filtered copper radiation (Kα = 1.5406) at 2θ range of 5˚–80˚. The crystallite sizes of the prepared materials were determined using the Scherrer equation from the data obtained from XRD patterns. The X-ray photoelectron spectroscopy (XPS) spectra were recorded in a PHI 5000 Versaprobe instrument using monochromated Al-Kα radiation (1,486.6 eV) at 100 W (18.0 kV). The Fourier transformation infrared (FTIR) spectra were obtained using a FTIR spectrophotometer (Impact 400D) and KBr pellets. Differential scanning calorimetry (DSC) and DTG thermograms were recorded using the instrument Model Setaram STA units in the range of 50–800˚C with temperature rise of 10˚C min^{-1}. The surface morphology and particles size of the samples were, respectively, studied using a Philips XL30 scanning electron microscope (SEM) (accelerating voltage: 0.5–30 kV [100 V steps] and 3–30 kV [1 kV steps]; SEM resolution: 2.0 and 5.0 nm at 1 kV; magnification range: 20X–1 × 10^6×), equipped with an energy dispersive analysis X-ray spectroscopy (EDAX), and Phillips CM10 transmission electron microscope (TEM) (40–100 kV accelerating voltage adjustable in 20 kV increments: ±60˚ specimen tilt; magnification range: 20–510,000×). The amount of iron was measured by an atomic absorption spectrometer, Perkin Elmer AAnalyst 300 (Air-C_2H_2, λ = 248 nm). Degradation efficiency was determined using UV–vis spectrophotometer (Carry 100 Scan) at the wavelength of maximum absorption of furfural and finally the degradation extent was proved by high-performance liquid chromatography (HPLC) (Agilent Technologies 1200 series) and chemical oxygen demand (COD). Measurements of total organic carbon (TOC) were performed by TOC analyzer (Shimadzu TOC-VCSN).

2.4. Photocatalytic experiments

In a typical degradation experiment, 0.2 g of FeO-CP was added to 50 mL of 10 times diluted wastewater solution containing 37.5 mmol/L furfural with initial pH of 8 at room temperature. Preliminary experiments showed that about 3.7% of furfural was removed by the surface adsorption during 30 min contact time and thereafter remained constant. Hence, before irradiation experiments, to fix the surface adsorption extent, the obtained suspensions were shaken for 30 min at dark. The aqueous suspensions were then irradiated with a UV lamp under magnetic stirring. The blank solution had the same conditions but without the photocatalyst. At regular time intervals, about 10 mL of suspensions were taken and centrifuged for 15 min to get a clear solution to record its absorbance at λ = 245 nm for the furfural. Degradation efficiency was determined using absorbance of solutions before and after irradiation process using the following equation:

$$\text{Degradation } \% = (A_0 - A/A_0) \times 100 \quad (1)$$

where A_0 is the absorbance of blank and A is the absorbance of sample after irradiation process.

3. Results and discussion

3.1. Characterization

3.1.1. XRD and XPS patterns

The XRD patterns of the pretreated CP (CP), Fe-CP (Fe-CP), and FeO-CP (FeO-CP) samples were recorded and the corresponding patterns are shown in Fig. 1(A). The more intense characteristic lines at 2θ values of 9.8˚, 11.2˚, 22.4˚, 26.0˚, and 30.0˚ observed from the XRD pattern of CP sample (pattern a in

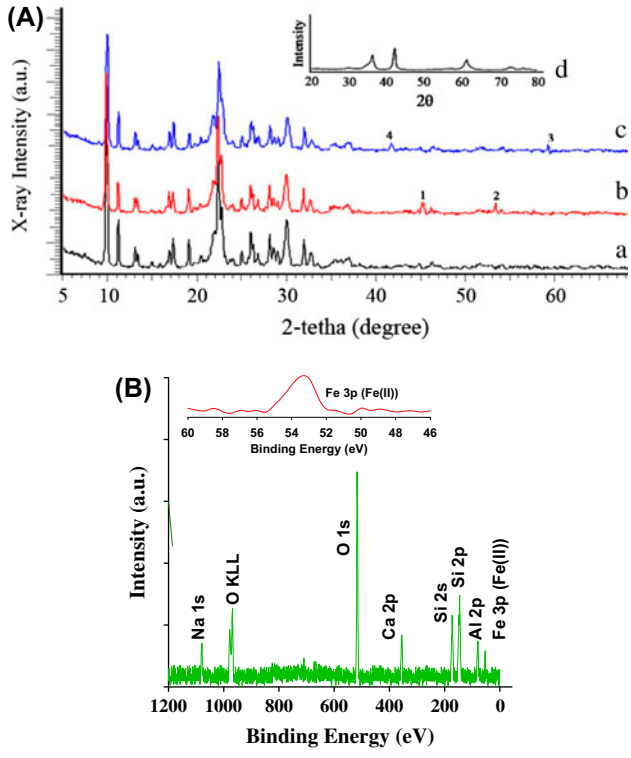

Fig. 1. (A) XRD patterns of CP (a), Fe-CP (b), and FeO-CP (c) (inset: XRD pattern of nano FeO particles with different particle sizes); (B) XPS spectrum of FeO-CP sample (inset: expanded Fe-peak in the range of 60–45 eV).

Fig. 1(A)) that show good agreement with the data of natural CP zeolite [12,17]. Presence of the weak peaks at 2-theta values of 44.9˚, 53˚ and also the peaks at 2-theta values of 41.9˚ and 59.8˚ in the Fe-CP and FeO-CP patterns, respectively (1 and 2 in pattern b, 3 and 4 in pattern c), which are absent in the CP pattern can consider for incorporation of Fe^{2+} and FeO in CP structure. Inset (d) in Fig. 1 shows the XRD pattern of nano FeO particles [18]. The weak peaks at 2-theta values of 41.9˚ and 59.8˚ in the FeO-CP pattern are in accordance with these results confirming formation of FeO nanoparticles in the zeolite channels due to their definite and nanometer pores of zeolites. Comparison of XRD patterns in Fig. 1(A) shows some changes at 2-theta range from 25˚ to 27˚ which can be considered as evidences for the incorporation of Fe(II) and FeO in the zeolite structure. The results illustrate that the intensity of lines for Fe-CP and FeO-CP are similar to the raw CP sample. On the other hand, the entrance of Fe and FeO to the structure of the zeolite did not change the original zeolite framework.

Crystallite size of powders was estimated using the following Scherrer's equation [8,9].

$$D = 0.9\lambda/\beta \cos\theta \quad (2)$$

where D is the crystallite size (nm), λ the radiation wavelength (0.15406 nm), θ the diffraction peak angle, and β is the corrected half-width at half-maximum intensity. The average particles sizes of CP, Fe-CP, and FeO-CP were obtained about 1.26, 1.32, and 1.52 μm, respectively.

To confirm what form of iron oxide has formed on CP particles during calcinations process, XPS experiment was done onto the calcinated sample and the corresponding graph is shown in Fig. 1(B). All characteristics peaks of CP have good agreement with the literature [19]. As shown one peak was only observed for Fe species at 54 eV. As reported in the literature [20], Fe(II) and Fe(III) cations have corresponding 3p peaks at 53.9 and 55.6 eV, respectively. As we know, FeO and Fe_2O_3 include Fe(II) and Fe(III) cations, respectively. Comparison of the results with literature confirms that the peak located at 54 eV belong to Fe(II) cations, confirming formation of FeO in the calcined sample.

3.1.2. FT-IR analysis

The infrared spectra of the CP, Fe-CP, and FeO-CP samples are shown in Fig. 2. The main characteristic bands of CP were found at the wavenumbers of 472, 609, 768, 1,077, and 1,639 cm^{-1}. The band located at 472 cm^{-1} belongs to the stretching vibrations of Al–O bond, while the bands located at 798 and 1,076 cm^{-1} belong to the Si–O–Si bond [21]. The vibration bands located at 1,639 (bending) and 3,600 cm^{-1} correspond to the zeolitic water [21,22]. FTIR spectra of samples were also used for studding the shifts due to incorporation of Fe(II) and FeO into the zeolite framework. Breck showed that by entering transition metal cations into a zeolitic structure, some slight shifts may happen in the peak positions for the peaks located at the right side of the T–O–T or O–T–O stretching vibrations (T = Al or Si) [23]. Such shifts can be observed in our results for Fe-CP and FeO-CP after ion exchange and calcination processes. The new peaks at 412, 422, and 431 cm^{-1} in the FeO-CP spectrum, which are absent in the CP spectrum, indicate the incorporation of Fe^{2+} in the zeolite. In addition, the slight shifts can be observed for the located peaks at 470, 608, 780, and 1,060 cm^{-1} in the spectrum of FeO-CP with respect to the CP spectrum. Similar shifts can also be observed for the located peaks at 469, 610, 788, and 1,068 cm^{-1} in the spectrum (b) that belongs to Fe-CP. We concluded that these shifts belong to entering of Fe^{2+} and FeO in the zeolite structure. Similar results have been observed in our previous works by incorporation of some transition metal cations and the corresponding sulfides or oxides into the different zeolites [24–26].

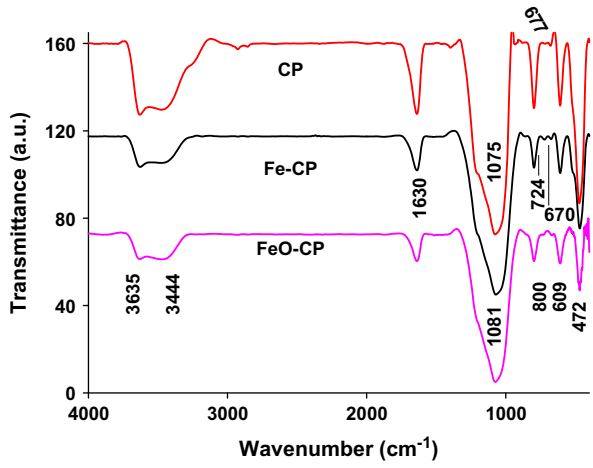

Fig. 2. FT-IR spectra of CP, Fe-CP, and FeO-CP.

3.1.3. SEM, TEM, and EDAX analysis

The surface morphology of CP, Fe-CP, and FeO-CP samples were studied by SEM and the corresponding SEM pictures are presented in Fig. 3. The

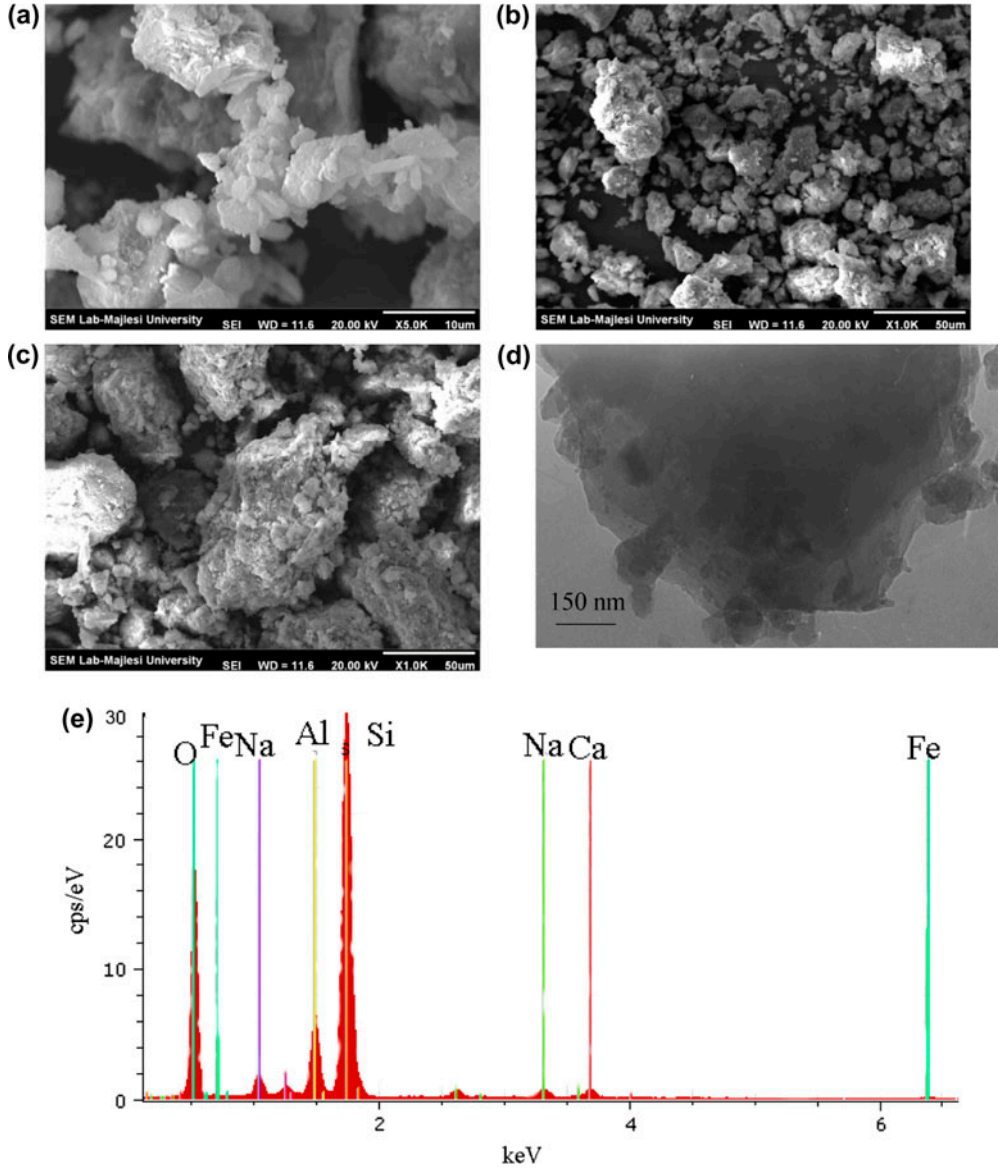

Fig. 3. SEM images of CP (a), Fe-CP (b), FeO-CP (c), TEM image (d), and EDAX spectrum of FeO (5%)-CP (e).

crystallites of the unloaded zeolite have very well-defined layer-like crystals. The images of the loaded samples also show the same crystals that indicate the zeolite crystallites have been not been affected by the Fe^{2+} and FeO loading. The average crystallite sizes of CP, Fe-CP, and FeO-CP powders were estimated about 1.67, 1.82, and 2.07 μm, respectively. As shown, the trend in the data of crystallite sizes is in coherence with the XRD data of crystallite sizes. Also, TEM image of FeO-CP is shown in Fig. 3(d). EDX spectrum of FeO-CP is also shown in Fig. 3(e). Based on EDX analysis, the following component percentages were obtained: Al_2O_3: 25%; SiO_2: 61%; FeO: 5.8%; CaO: 1.4%; Na_2O: 0.9%.

3.1.4. Thermal analysis

Thermal characteristics of samples were analyzed by using the TG/DTG and DSC techniques. The samples were heated in a platinum crucible over the temperature range of 50–800 ℃ with a heating rate of 10 ℃ min^{-1} in the nitrogen atmosphere, of which the results are shown in Fig. 4. The aim of this study is analyzing changes resulted in heating treatment of zeolite which have affected by ion exchange and calcination processes. On the other hand, the changes in the thermal behavior of samples confirm entering of Fe^{2+} ion and formation of FeO in CP structure. Comparison of the thermal patterns of the samples

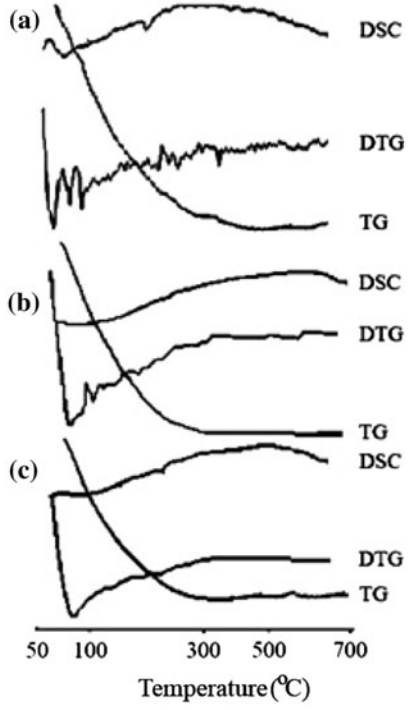

Fig. 4. Thermal analysis curves of CP (a), Fe-CP (b), and FeO-CP (c).

shows that there are no considerable changes in the zeolite phase. Comparison of TG/DTG curves in Fig. 4, shows that the total weight losses of about 11.2, 15.6, and 9.1%, respectively, happened for CP, Fe-CP, and FeO-CP samples at 80°C. The smaller weight loss of the raw CP sample with respect to Fe-CP shows lower hydration of original zeolitic cations (predominantly Na^+ and Ca^{2+}) with respect to entered Fe^{2+} cations. Our results agree with the weigh loss of Fe-exchanged CP in literature [27]. The weight loss trend, which is gained from TG and DTG fluctuations, is also viewed in DSC curves by observing the endothermic processes during the temperature programing.

3.1.5. UV–vis diffuse reflectance spectroscopy

The UV–vis diffuse reflectance spectroscopy (DRS) results of the used samples are shown in Fig. 5. In the raw CP sample, spectral maxima appeared around 255 nm in UV region. While, in the Fe-CP curve, a red shift was observed toward 290 nm and two maximum were also observed at 320 and 490 nm. We suggest that these bands belong to Fe-bonded to oxygen atoms of zeolite framework. These observations show the entering of Fe cations into the zeolite structure during

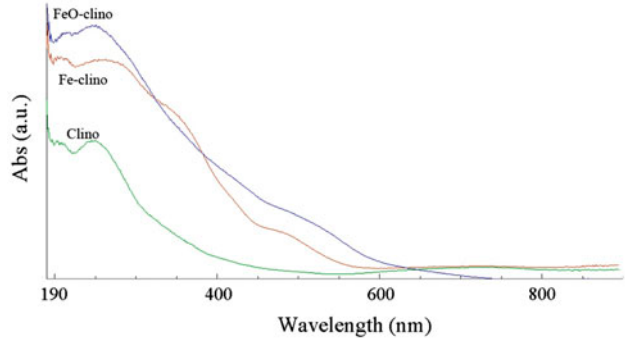

Fig. 5. DRS results of CP, Fe-CP, and FeO-CP samples.

the ion exchange process. DRS spectrum of FeO-CP shows an increase in absorbance of the obtained composite. In the spectra of Fe-CP and FeO-CP new absorption bands present about 500 nm which relate to transitions of FeO. On the other hand, Fe cations bonded to framework oxygens of CP and formed FeO can absorb visible photons. In general, the results of XRD, FT-IR, TG/DTG, and DRS confirm sufficient loading of FeO into the CP structure. In addition to instrumental studies, the dark white color of the Fe-CP sample changed to dark red color after calcination process which can be considered as a primary evidence for changing of Fe(II) to FeO and formation of the FeO-CP catalyst.

3.2. Catalytic activity of FeO-CP sample

3.2.1. Effect of zeolite

Heterogeneous photocatalytic reactions were performed by FeO, CP, and FeO-CP samples at similar experimental conditions as: pH 8 (natural pH of solution), 0.2 g suspended catalyst in 50 mL wastewater solution containing 37.5 mmol/L furfural under 180 min Hg-lamp irradiation (Fig. 6). As shown in Fig. 6, FeO alone showed smaller degradation rate while the FeO-CP displayed higher photocatalytic activity than the bulk FeO. This may be caused by the high adsorption capability of the zeolite support toward furfural molecules. On the other hand, it maybe that some of the zeolite pores and cavities are still open even after the loading of FeO, which enables the FeO-CP to keep the adsorption ability to some extent [28]. Thus, the FeO-CP is more efficient than the pure FeO due to its remarkable ability in gathering the organic substance near to the FeO particles. These results also showed that FeO particles loaded on the zeolite are active centers for the degradation of pollutant. The obtained results showed that the FeO out of

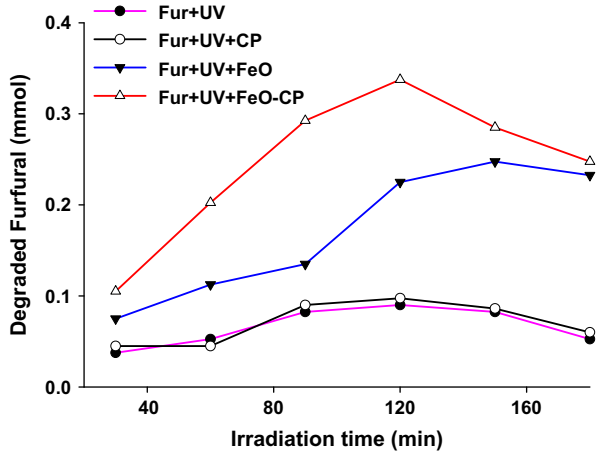

Fig. 6. Effect of zeolite on the FeO photocatalytic activity; 4 g/L^{-1} of the catalyst; initial solution pH 8, initial furfural concentration, 37.5 mmol/L.

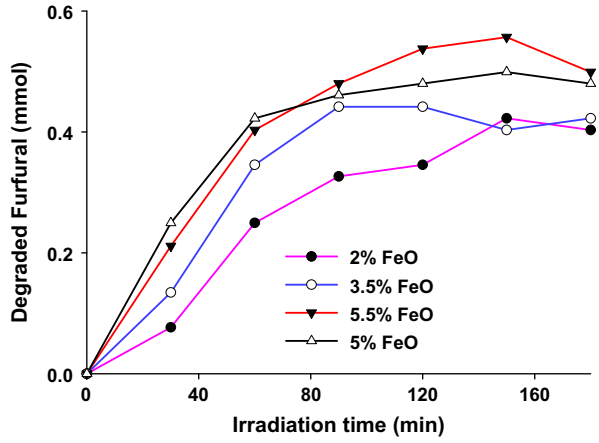

Fig. 7. Effect of FeO loaded on the zeolite in the degradation of furfural in wastewater; 1 g/L^{-1} of the catalyst; initial solution pH 8, initial furfural concentration, 375 mmol/L.

the zeolite does not have considerable degradation efficiency for furfural in the wastewater. These results are in agreement with literature [12,24–26].

3.2.2. Effect of FeO loading

The extent of loaded FeO as the active centers of the proposed catalyst affects the efficiency of the photodegradation process due to generation of sufficient electron–hole pairs. Hence, the effect of the amount of doped FeO on the performance of the proposed catalysts was investigated. Three catalysts were prepared by ion exchanging of CP in 0.1, 0.2, and 0.5 mol/L of Fe^{2+} aqueous solutions with FeO contents of 35, 55, 70 mg/g of the catalysts (based on the atomic absorption results of Fe determination), respectively. To study the effect of the amount of loaded FeO on the degradation extent of furfural, some experiments were carried out by these catalysts in the similar operational conditions (natural pH 8, 1 g/L^{-1} of the catalysts, initial concentration of furfural in wastewater 375 mmol/L, irradiation time of 180 min). As shown in Fig. 7, there is no considerable difference between the degradation efficiency of the catalysts containing 55 and 70 mg FeO per gram of the catalysts. These results are in opposition with our expectations. On the other hand, it would be expected that with increase in the FeO loading, more electron–hole pairs should be produced and hence the efficiency of the process should increase. We observed the same results in our previous work; so, by increasing in the CuO loaded onto zeolite X, the photo-efficiency of the used catalyst toward photodecolorization of methylene blue was decreased [25]. We suggested that with increase in the active CuO component, the number of active sites on the catalyst surface and hence the production of hydroxyl radicals tends to increase. But at high active component values, aggregation of semiconductor particles onto the surface of zeolite causes a decrease in the effective surface area of the catalyst and hence decolorization efficiency tends to decrease. Moreover, at higher semiconductor loading, collision of the excited molecules with ground state one deactivates the excited semiconductor molecules which finally led to decrease in the degradation efficiency.

The plot of ln C_0/C vs. time as a function of catalyst loading was plotted to calculate the rate constants based on its linear segment and the results are collected in Table 2. This will be discussed in more details in the investigation of the effect of furfural concentration in the next sections.

3.2.3. Effect of catalyst concentration

Catalyst loading is an important factor which can significantly influence the photocatalytic degradation rate [25]. Hence, the effect of catalyst dosage in the range of 0.04–6 g/L^{-1} was studied of which the results are shown in Fig. 8. It can be seen that the initial slopes of the curves were increased greatly by increasing the catalyst loading from 0.04 to 4 g/L^{-1} and thereafter remained constant or decreased. The increase in the catalyst amount actually increases the number of active sites on the surface of the photocatalyst, thus causing an increase in the number of produced •OH radicals [29,30]. But, due to an increase in turbidity of the suspension because of the high dose of the catalyst, penetration of photons decreases which

Table 2
Reaction rate constants of furfural degradation as a function of various experimental parameters

Investigated parameter	Value	$\kappa \times 10^{-4}$ (min^{-1})
Catalyst mass (g/L^{-1})	0	3
	0.04	5
	0.4	8
	2.0	16
	4.0	23
	6.0	20
Concentration of furfural (mmol/L)	18.75	50
	37.5	50
	75.0	24
	187.5	26
	375	22
pH of solution	3	15
	5	30
	8	46
	11	32
Concentration of H_2O_2 (mmol/L)	0	48
	25	50
	[a]50	12
	[b]50	24
	[c]50	99
	100	62
	150	52
Concentration of $KBrO_3$ (mg/L)	0	41
	10	44
	25	58
	[a]50	10
	[b]50	24
	[c]50	101
	100	70

[a]Experiment was carried out in the presence of only H_2O_2 or $KBrO_3$ at dark.
[b]Experiment was carried out in the presence of only H_2O_2 or $KBrO_3$ under irradiation.
[c]Experiment was carried out in the presence of H_2O_2 or $KBrO_3$ and catalyst under irradiation.

in turn decreases the photoactivated volume of the suspended catalyst [31]. Thus, it can be concluded that higher dose of the catalyst may not be useful due to negative effects of aggregation and light scattering. Therefore, the catalyst dose of 4 g/L^{-1} was used in next studies. This value is very high with respect to used catalyst doses in common synthetic solutions containing pure pollutants (0.05–1 g/L^{-1}) [9,12,24–26]. We believe that in the used wastewater a higher adsorbed species on the catalyst surface surrounds FeO centers. This causes a significant decrease in the activated semiconductor molecules and finally the electron–hole generation. In addition, due to adsorption of other pollutants onto the catalyst surface, less furfural molecules can reach near the catalyst surface where the hydroxyl radicals can be produced. Hence, the efficiency of the degradation process tends to decrease.

3.2.4. Effect of concentration of furfural in wastewater

In preliminary studies, concentration of furfural in the used wastewater was determined. For this purpose, standard addition method was used to reduce any matrix effects on the furfural determination. Based on the measurement of absorbance of samples at 245 nm by UV/V is spectrophotometer, the concentration of furfural in the original wastewater was obtained about 375 mmol/L.

The concentration of pollutants is an important parameter in the photodegradation treatments. Fig. 9 shows the effect of concentration of furfural (from 18.75 to 375 mmol/L) on the efficiency of the process. As shown, degradation efficiency tends to increase by increasing the concentration from 18.75 to 37.5 mmol/L furfural and thereafter tends to decrease. At high diluted samples (lower concentrations), lesser furfural

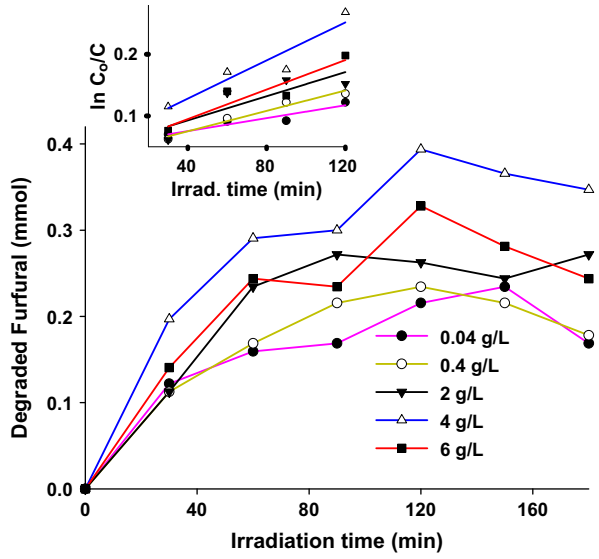

Fig. 8. Effect of FeO-CP dosage on the degradation efficiency; initial furfural concentration in wastewater, 375 mmol/L; initial pH 8.

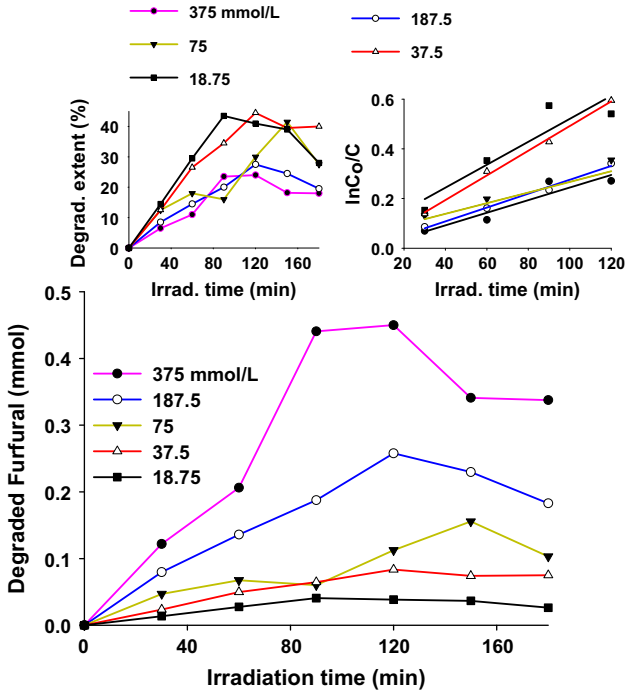

Fig. 9. Effect of the initial concentration of furfural on the degradation efficiency; 4 g L^{-1} of the catalyst; initial solution pH 8, inset 1: degradation percentages and inset 2: ln C_0/C plots.

molecules can reach near the catalyst surface and hence the produced hydroxyl radicals tend to deactivate before they can react with furfural molecules. At high concentrate samples, due to absorption of large amounts of photons by furfural or other present pollutants, lesser FeO particles can excite and finally the degradation efficiency tends to decrease. This in turn confirms the small role of direct photolysis for furfural degradation in the used conditions. The kinetic analysis under different concentrations of furfural was also investigated and the obtained results are depicted in the first inset of Fig. 9. Kinetics of the photocatalytic reactions follows the following Langmuir–Hinshelwood model [5,32]:

$$r = \mathrm{d}C/\mathrm{d}t = k \cdot KC/1 + \mathrm{KC} \tag{3}$$

where r is the degradation rate of pollutant (mg/L^{-1} min^{-1}) after the illumination time of t (min), C the concentration of the reactant (mg/L^{-1}), k the reaction rate constant (mg/L^{-1}), and K the Langmuir–Hinshelwood adsorption equilibrium constant (L mg^{-1}). When the initial concentration (C_0) is about millimolar (too small C_0), the equation can be simplified to an apparent pseudo- first-order rate equation as follows:

$$\ln C_0/C = kKt \tag{4}$$

From the linear segment of the plots of ln C_0/C vs. time, indicating the pseudo-first-order kinetic expression [33], the rate constants as a function of the initial concentration of furfural in the wastewater sample were calculated and the results are summarized in Table 2.

Here, the effect of the concentration on the degradation efficiency will be discussed in another point of view. We calculated the efficiency of the process in terms of the mmoles of degraded furfural and the obtained results are shown in the second inset of Fig. 9. Based on degradation percentage results, a solution of 37.5 mmol/L furfural showed a better efficiency while the better results were obtained based on the mmoles of the degraded furfural in a 375 mmol/L furfural solution. According to the results, the maximum degradation percents of 45 and 25% were obtained for the solutions containing 37.5 and 375 mmol/L of furfural during 120 min irradiation, respectively. On the other hand, degradation of 25% of 375 mmol/L of furfural shows higher millimoles of the degraded furfural molecules. Hence, we suggest that it is better to report efficiency of the photodegradation processes in terms of the millimoles of the degraded pollutants (instead of degradation%). Because, in the preliminary studies we calculated degradation percentages (instead of degraded

mmoles), 37.5 mmol/L of the pollutant was used in the next studies.

3.2.5. Effect of pH

To study the effect of pH on the degradation efficiency, some experiments were carried out by using 37.5 mmol/L furfural wastewater suspensions containing 4 g L^{-1} FeO-CP catalyst at pH values of 3, 5, 8, 11. As shown in Fig. 10, the degradation rate was increased with increase in the pH from 3 to 8 and thereafter decreased. In acidic pH media, the anion Cl^- reacts with hydroxyl radicals, leading to yield inorganic radical ions (ClO^-). These inorganic radical anions show a much lower reactivity than $^\bullet OH$, so that they do not take part significantly in the furfural degradation. There is also a drastic competition between furfural and chloride anions with respect to $^\bullet OH$. Hence, an increase in pH till a definite level can increase the degradation efficiency [9]. Decrease in the degradation efficiency at higher pH values may be because of formation of $HO_2^\bullet$ radicals due to the reaction of $^\bullet OH$ with ^-OH. The reactivity of these radicals with organic materials is lower than $^\bullet OH$ [34,35]. Based on the inset of Fig. 10, the rate constant values (k, min^{-1}) as a function of pH were calculated and presented in Table 2.

3.2.6. Effect of H_2O_2

To determine the influence of hydrogen peroxide in the photodegradation efficiency of furfural, some experiments were carried out at different hydrogen peroxide concentrations including 25, 50, 100, and 150 mmol/L by using the similar operational conditions (pH 8, 4 g/L^{-1} FeO-CP and 37.5 mmol/L of furfural) (Fig. 11). As shown, the degradation rate was increased with increasing the hydrogen peroxide dose to 50 mmol/L and thereafter decreased. In a photodegradation reaction, hydrogen peroxide critically affects the degradation efficiency of pollutants because it directly affects the number of produced $^\bullet OH$ radicals [36,37]. At high concentrations, the adsorbed hydrogen peroxide on the surface of the photocatalyst could effectively scavenge the $^\bullet OH$ radicals formed on the surface causing $HO_2^\bullet$ radicals to form, which are less reactive than $^\bullet OH$ [36]. However, in the presence of hydrogen peroxide, the following equations take place and affect the degradation efficiency:

$$e^- \ CB + H_2O_2 \rightarrow OH^- + {}^\bullet OH \quad (5)$$

$$O_2^{\bullet -} + H_2O_2 \rightarrow OH^- + {}^\bullet OH + O_2 \quad (6)$$

$${}^\bullet OH + H_2O_2 \rightarrow H_2O + HO_2^\bullet \quad (7)$$

$$HO_2^\bullet + {}^\bullet OH \rightarrow H_2O + O_2 \quad (8)$$

Inset of Fig. 11 shows the plot of ln (C/C_0) vs. time as a function of concentration of hydrogen peroxide. The rate constants (k, min^{-1}) as a function of H_2O_2 concentration on the degradation process are also summarized in Table 2.

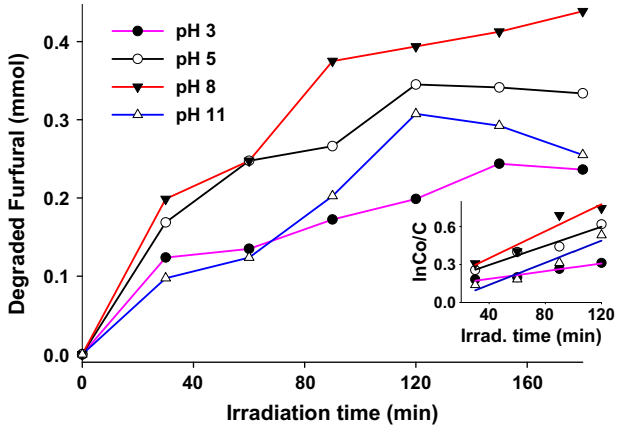

Fig. 10. Effect of solution pH on the degradation efficiency of furfural; 4 g L^{-1} of the catalyst; initial furfural concentration, 37.5 mmol/L.

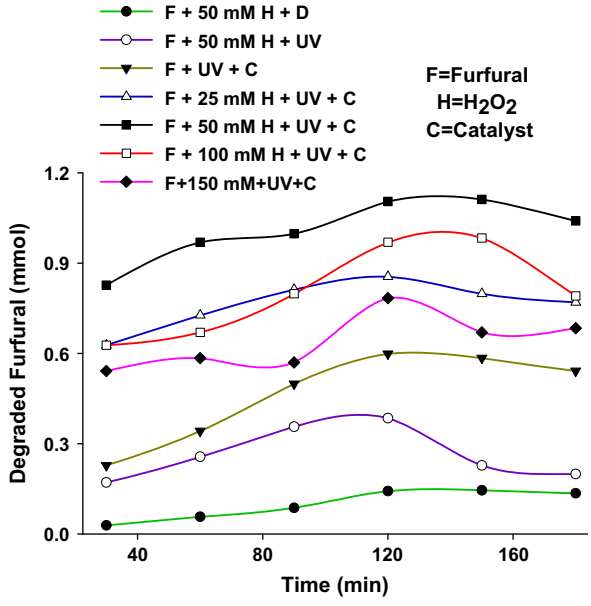

Fig. 11. Effect of the hydrogen peroxide concentration on degradation efficiency of furfural; 4 g L^{-1} of the catalyst; initial solution pH 8; initial furfural concentration, 37.5 mmol/L.

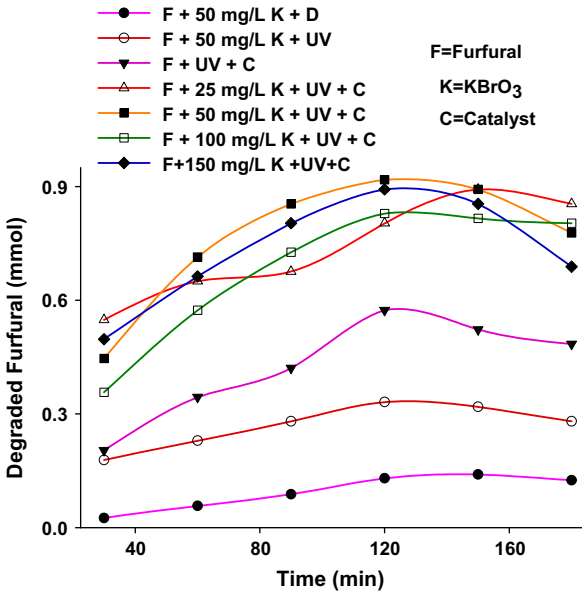

Fig. 12. Effect of the potassium bromate concentration on the degradation efficiency of furfural; 4 g/L^{-1} of the catalyst; initial solution pH 8; initial furfural concentration, 37.5 mmol/L.

3.2.7. Effect of $KBrO_3$

Fig. 12 shows the degradation rate of a 37.5 mmol/L furfural wastewater in the presence of FeO-CP (4 g L^{-1}) as a function of potassium bromate dose (10, 25, 50, and 100 mg/L). As shown, by increasing the potassium bromate dose from 10 to 25 mg/L, the degradation rate was increased. The enhancement of the removal rate is due to the reaction between BrO_3^- ion and conduction band electron (Eqs. (9) and (10)), which reduces the electron–hole recombination.

$$BrO_3^- + 2H^+ + e_{CB}^- \rightarrow BrO_2^{\bullet} + H_2O \quad (9)$$

$$BrO_3^- + 6H^+ + 6e_{CB}^- \rightarrow (BrO_2^-, HOBr) \rightarrow Br^- + 3H_2O \quad (10)$$

With further increase in the potassium bromate dose from 50 to 100 mg/L, the degradation rate was decreased. This is due to the adsorption of Br^- ions on the surface of FeO-CP, which affects the activity of the FeO-CP [38,39].

3.2.8. Mineralization studies of furfural

To confirm the degradation of furfural in the proposed wastewater sample, the obtained results were checked by using HPLC and COD methods. HPLC is a good technique to monitor the change in the concentration of organic compounds in a photodegradation process [40]. The degradation experiment was carried out at the optimum conditions including 4 g/L^{-1} of FeO-CP, 37.5 mmol/L furfural at pH 8 during 120 min irradiation. The samples before and after photodegradation process were studied by HPLC with a solvent phase consisted of water–acetonitryl mixture. The concentration of furfural in both samples was monitored by considering their peak intensities as shown in Fig. 13. The intensity of the peak was decreased gradually during the degradation process.

Because the reduction of COD reflects the extent of degradation or mineralization of pollutant species, the change in COD was also studied for confirming the degradation extent during the photodegradation experiments. Degradation experiments were performed under the above-mentioned optimum conditions over the period of 30–120 min of irradiation process. The COD was determined after separation of the FeO-CP catalyst by centrifuging the suspension, according to the standard method [41] and the corresponding results are shown in Fig. 14. As shown, the photocatalysis with FeO-CP is more efficient than the direct photolysis to decrease COD of the sample. The COD of sample was decreased during the photodegradation process, so 45% decrease in the COD (initial COD of sample = 134 mg/L^{-1}) was observed at the end of the process.

To confirm the complete degradation of pollutants present in the wastewater sample, photodegradation of a sample was studied under the optimized conditions and the reduction of TOC was followed. The initial TOC of 14,550 mg/L^{-1} of the subjected sample was decreased to 980, 698, and 415 mg/L^{-1} at irradiation times of 60, 90, and 120 min, respectively. These

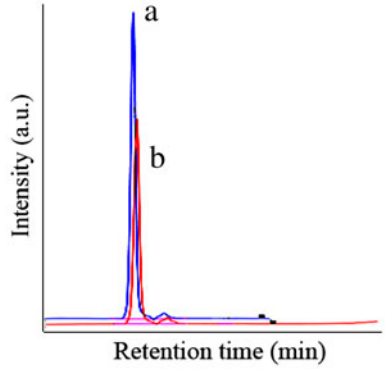

Fig. 13. HPLC chromatogram of the wastewater solution with (wastewater solution initial concentration = 37.5 mmol/L, FeO-CP = 4 g/L^{-1}, at pH 8, at 120 min of irradiation).

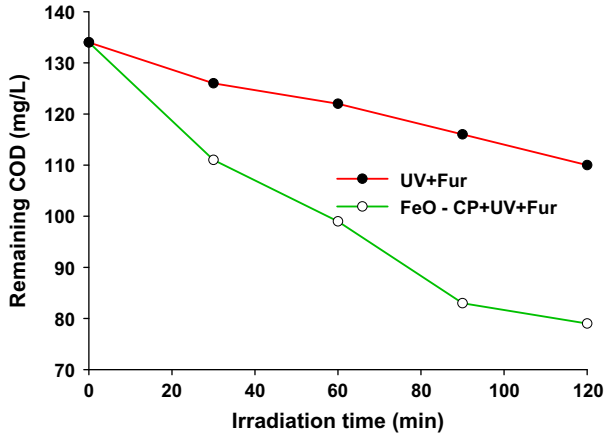

Fig. 14. COD values measured at different times for wastewater solution containing furfural with FeO-CP/UV, UV at (wastewater solution initial concentration = 37.5 mmol/L, FeO-CP = 4 g/L^{-1}).

values correspond to degradation extents of 32, 52, and 71% which are greater than the values obtained by spectrophotometric measurements. On the other hand, in spectrophotometric measurements, because of measurement of absorbance of samples at maximum absorption wavelength of furfural, only the degraded furfural molecules were measured. But, TOC results confirm that in addition of degradation of furfural molecules, other organic molecules present in the waste sample can also be degraded by the proposed catalyst. Hence, the proposed catalyst can be used for effective removal of the pollutants present in the proposed wastewater sample.

Finally, the results of HPLC, COD, and TOC analysis confirm the degradation of furfural in the used wastewater sample in the presence of the proposed photocatalyst under Hg-lamp irradiation.

4. Conclusion

The results of this study showed successful degradation of furfural in the proposed wastewater sample during a photocatalytic process. FeO doped onto the CP zeolite was the active center at the proposed FeO-CP catalyst, so the FeO or CP alone showed smaller degradation efficiency. The results also showed requirement of higher doses of photocatalyst for wastewater treatments. This is due to the high adsorbed species onto the surface of the catalyst in a wastewater sample which deactivates the active centers of the catalyst and decreases the adsorption of furfural by the catalyst. We suggest if the mmoles of the degraded pollutants was considered instead of its degradation % in a typical photodegradation process, much real results will be obtained. The presence of hydrogen peroxide and also potassium bromate increased the efficiency of the proposed method. The results showed a better efficiency of bromate than hydrogen peroxide because smaller amount of bromate was used to obtain same degradation level. COD and HPLC results are in accordance with the UV/V is degradation results, which confirm the usefulness of the proposed method in the photodegradation of the used wastewater sample.

References

[1] A. Dhir, N.T. Prakash, D. Sud, Comparative studies on TiO_2/ZnO photocatalyzed degradation of 4-chlorocatechol and bleach mill effluents, Desalin. Water Treat. 46 (2012) 196–204.
[2] S.M. Borghei, S.N. Hosseini, Comparison of furfural degradation by different photooxidation methods, Chem. Eng. J. 139 (2008) 482–488.
[3] A. Nageswara Rao, B. Sivasankar, V. Sadasivam, Kinetic study on the photocatalytic degradation of salicylic acid using ZnO catalyst, J. Hazard. Mater. 166 (2009) 1357–1361.
[4] R.A. Motiyenko, E.A. Alekseev, S.F. Dyubko, Microwave spectroscopy of furfural in vibrationally excited states, J. Mol. Spectrosc. 244 (2007) 9–12.
[5] M. Faramarzpour, M. Vossoughi, M. Borghei, Photocatalytic degradation of furfural by titania nanoparticles in a floating-bed photoreactor, Chem. Eng. J. 146 (2009) 79–85.
[6] U.K. Ghosh, N.C. Pradhan, B. Adhikari, Pervaporative separation of furfural from aqueous solution using modified polyurethaneurea membrane, Desalination 252 (2010) 1–7.
[7] M. Anbia, N. Mohammoadi, A nanoporous adsorbent for removal of furfural from aqueous solutions, Desalination 249 (2009) 150–153.
[8] J.K. Yang, S.M. Lee, M. Farrokhi, O. Giahi, M. Shirzad Siboni, Photocatalytic removal of Cr(VI) with illuminated TiO_2, Desalin. Water Treat. 46 (2012) 375–380.
[9] M.R. Samarghandi, J.K. Yang, S.M. Lee, O. Giahi, M. Shirzad-Siboni, Effect of different type of organic compounds on the photocatalytic reduction of Cr(VI) in presence of ZnO nanoparticles, Desalin. Water Treat. 52 (2014) 1531–1538.
[10] A. Nezamzadeh-Ejhieh, Z. Shams-Ghahfarokhi, Photodegradation of methyl green by nickel-dimethylglyoxime/ZSM-5 zeolite as a heterogeneous catalyst, J. Chem. 2013 (2013) 1–11 (Article ID 104093).
[11] A. Nezamzadeh-Ejhieh, M. Khorsandi, Photodecolorization of eriochrome black T using NiS–P zeolite as a heterogeneous catalyst, J. Hazard. Mater. 176 (2010) 629–637.
[12] A. Nezamzadeh-Ejhieh, S. Moeinirad, Heterogeneous photocatalytic degradation of furfural using NiS-clinoptilolite zeolite, Desalination 273 (2011) 248–257.
[13] H. Kazemian, H. Modarress, M. Kazemi, F. Farhadi, Synthesis of submicron zeolite LTA particles from natural clinoptilolite and industrial grade chemicals

using one stage procedure, Powder Technol. 196 (2009) 22–25.
[14] B. Calvo, L. Canoira, F. Morante, J.M. Martnez-Bedia, C. Vinagre, J.E. Garcia-Gonzalez, J. Elsen, R. Alcantara, Continuous elimination of Pb^{2+}, Cu^{2+}, Zn^{2+}, H^{+} and NH_4^{+} from acidic waters by ionic exchange on natural zeolites, J. Hazard. Mater. 166 (2009) 619–627.
[15] E.L. Lopes, G.J.P. Abreu, R. Paniago, E.A. Soares, V.E. de Carvalho, H.-D. Pfannes, Atomic geometry determination of FeO(001) grown on Ag(001) by low energy electron diffraction, Surf. Sci. 601 (2007) 1239–1245.
[16] F.B. Li, X.Z. Li, X.M. Li, T.X. Liu, J. Dong, Heterogeneous photodegradation of bisphenol A with iron oxides and oxalate in aqueous solution, J. Colloid Interface Sci. 311 (2007) 481–490.
[17] M. Nikazar, K. Gholivand, K. Mahanpoor, Photocatalytic degradation of azo dye Acid Red 114 in water with TiO_2 supported on clinoptilolite as a catalyst, Desalination 219 (2008) 293–300.
[18] Y. Hou, Z. Xu, Sh. Sun, Controlled synthesis and chemical conversions of FeO nanoparticles, Angew. Chem. Int. Ed. 46 (2007) 6329–6332.
[19] D. Ruiz-Serrano, M. Flores-Acosta, E. Conde-Barajas, D. Ramirez-Rosales, J.M. Yanez-Limon, R. Ramirez-Bon, Study by XPS of different conditioning processes to improve the cation exchange in clinoptilolite, J. Mol. Struct. 980 (2010) 149–155.
[20] T. Yamashita, P. Hayes, Effect of curve fitting parameters on quantitative analysis of $Fe_{0.94}O$ and Fe_2O_3 using XPS, J. Electron. Spectrosc. Relat. Phenom. 152 (2006) 6–11.
[21] M.L. Chveza, L. De Pablob, T.A. Garcia, Adsorption of Ba_2^{+} by Ca-exchange clinoptilolite tuff and montmorillonite clay, J. Hazard. Mater. 175 (2010) 216–223.
[22] K.O. Xavier, J. Chacko, K.K. Mohamed Yusuff, Zeolite-encapsulated Co(II), Ni(II) and Cu(II) complexes as catalysts for partial oxidation of benzyl alcohol and ethylbenzene, Appl. Catal. A 258 (2004) 251–259.
[23] D.W. Breck, Zeolite Molecular Sieves: Structure, Chemistry and Uses, John Wiley & Sons, New York, NY, 1974.
[24] A. Nezamzadeh-Ejhieh, M. Khorsandi, Heterogeneous photodecolorization of Eriochrome Black T using Ni/P zeolite catalyst, Desalination 262 (2010) 79–85.
[25] A. Nezamzadeh-Ejhieh, S. Hushmandrad, Solar photodecolorization of methylene blue by CuO/X zeolite as a heterogeneous catalyst, Appl. Catal. A 388 (2010) 149–159.
[26] A. Nezamzadeh-Ejhieh, Z. Salimi, Heterogeneous photodegradation catalysis of o-phenylenediamine using CuO/X zeolite, Appl. Catal. A 390 (2010) 110–118.
[27] M.K. Doula, Synthesis of a clinoptilolite–Fe system with high Cu sorption capacity, Chemosphere 67 (2007) 731–740.
[28] M. Alvaro, E. Carbonell, M. Espla, H. Garcia, Iron phthalocyanine supported on silica or encapsulated inside zeolite Y as solid photocatalysts for the decolorization of phenols and sulfur heterocycles, Appl. Catal. B 57 (2005) 37–42.
[29] M.A. Rauf, S.S. Ashraf, Fundamental principles and application of heterogeneous photocatalytic degradation of dyes in solution, Chem. Eng. J. 151 (2009) 10–18.
[30] M.H. Habibi, H. Vosooghian, Photocatalytic degradation of some organic sulfides as environmental pollutants using titanium dioxide suspension, J. Photochem. Photobiol. A 174 (2005) 45–52.
[31] A. Nezamzadeh-Ejhieh, Z. Banan, Kinetic investigation of photocatalytic degradation of dimethyldisulfide by zeolite A containing nano CdS, Iran. J. Catal. 2(2) (2012) 77–81.
[32] Y. Zhang, H. Wu, J. Zhang, H. Wang W. Lu, Enhanced photodegradation of pentachlorophenol by single and mixed cationic and nonionic surfactants, J. Hazard. Mater. 221–222 (2012) 92–99.
[33] A. Nezamzadeh-Ejhieh, M. Karimi-Shamsabadi, Decolorization of a binary azo dyes mixture using CuO incorporated nanozeolite-X as a heterogeneous catalyst and solar irradiation, Chem. Eng. J. 228 (2013) 631–641.
[34] A. Nezamzadeh-Ejhieh, M. Amiri, CuO supported Clinoptilolite towards solar photocatalytic degradation of p-aminophenol, Powder Technol. 235 (2013) 279–288.
[35] M.B. Kasiri, H. Aleboyeh, A. Aleboyeh, Decolorization of Acid Blue 74 using Fe-ZSM5 zeolite as a heterogeneous photo-Fenton catalyst, Appl. Catal. B 84 (2008) 9–15.
[36] A. Nezamzadeh-Ejhieh, K. Shirvani, CdS loaded an Iranian Clinoptilolite as a heterogeneous catalyst in photodegradation of *p*-aminophenol, J. Chem. 2013 (2013) 1–11 (Article ID 541736).
[37] K.A. Halhouli, Effect of pH and temperature on degradation of dilute dihydroxybenzene, in aqueous titanium dioxide suspension irradiated by UV light, J. Photochem. Photobiol. A 200 (2008) 421–425.
[38] N. Sobana, M. Swaminathan, The effect of operational parameters on the photocatalytic degradation of Acid Red 18 by ZnO, Sep. Purif. Technol. 56 (2007) 101–107.
[39] A. Syoufian, K. Nakashima, Degradation of methylene blue in aqueous dispersion of hollow titania photocatalyst: Study of nt by various electron scavengers, J. Colloid Interface Sci. 317 (2008) 507–512.
[40] J. Fiori, R. Gotti, C. Bertucci, V. Cavrini, Investigation on the photochemical stability of lercanidipine and its determination in tablets by HPLC–UV and LC–ESI–MS/MS, J. Pharm. Biomed. Anal. 41 (2006) 176–181.
[41] American Public Health Association, Standard Methods for the Examination of Water and Wastewater, eighteenth ed., New York, NY, 1992.